

Supping Information

Facile synthesis of 3D porous $\text{Co}_3\text{V}_2\text{O}_8$ nanoroses and 2D $\text{NiCo}_2\text{V}_2\text{O}_8$ nanoplates with high performance surpercapacitor and electrocatalytic oxygen evolution reaction properties

Jingchao Zhang,^a Baiqing Yuan,^a Shufang Cui,^a Nana Zhang,^a Jingjing Wei,^a Xiao Wang,^a Daojun Zhang*,^a Renchun Zhang*^a and Qisheng Huo^b

^aHenan Province Key Laboratory of New Opto-electronic Functional Materials, College of Chemistry and Chemical Engineering, Anyang Normal University, Anyang, 455000, Henan, China

^b State Key Laboratory of Inorganic Synthesis and Preparative Chemistry, College of Chemistry, Jilin University, Changchun 130012, China

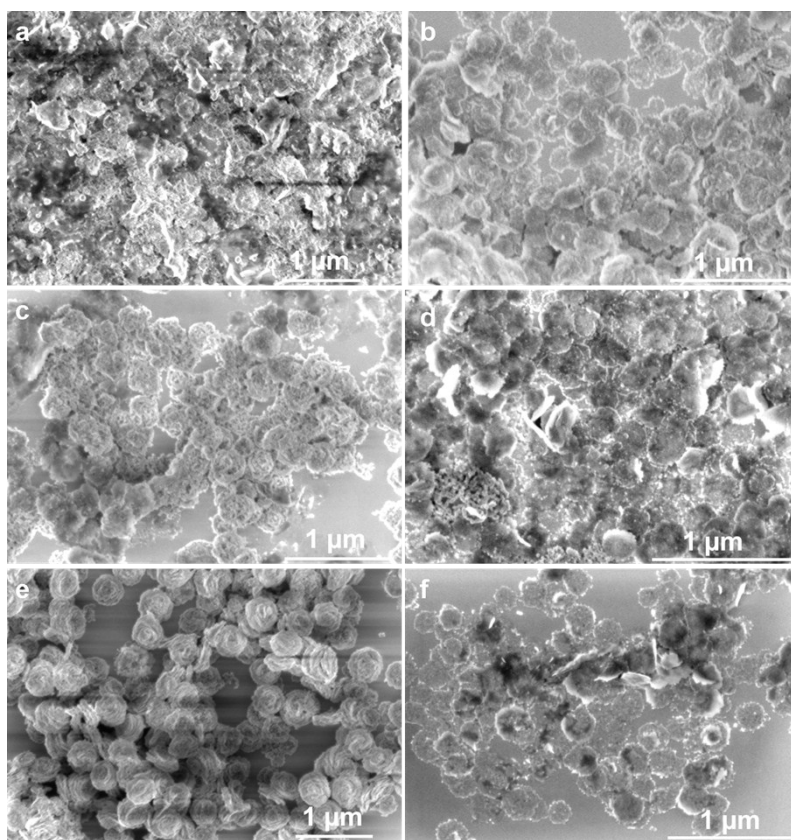


Fig.S1 SEM images of $\text{Co}_3\text{V}_2\text{O}_8$ and $\text{NiCo}_2\text{V}_2\text{O}_8$ obtained at different reaction time. (a-b) 3 h, (c-d) 6 h, (e-f) 9 h.

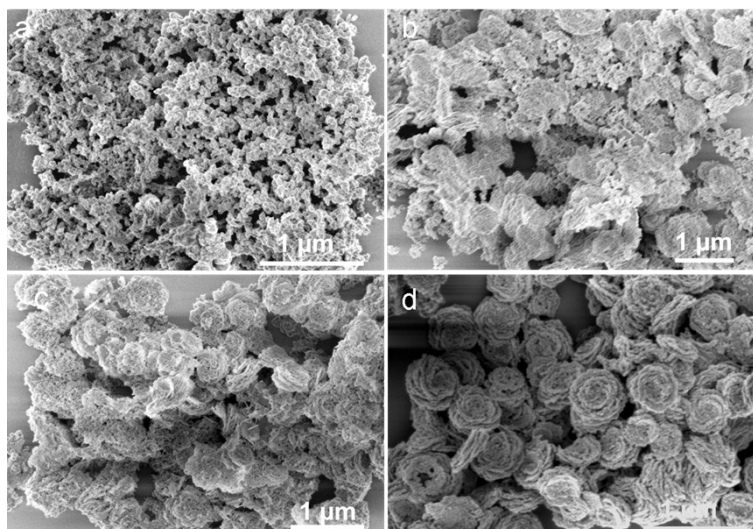


Fig. S2 SEM images of $\text{Co}_3\text{V}_2\text{O}_8$ obtained at different amount of methanol. (a) 0 mL, (b) 1.5 mL, (c) 3.0 mL, (d) 4.5 mL.

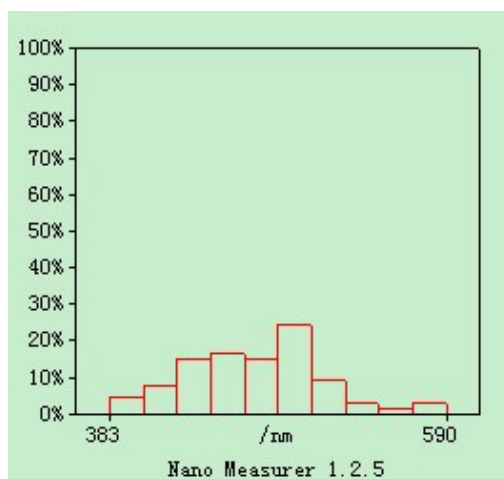


Fig. S3 The particle size histogram of synthesized $\text{Co}_3\text{V}_2\text{O}_8$ nanoroses obtained from Fig. 1a.

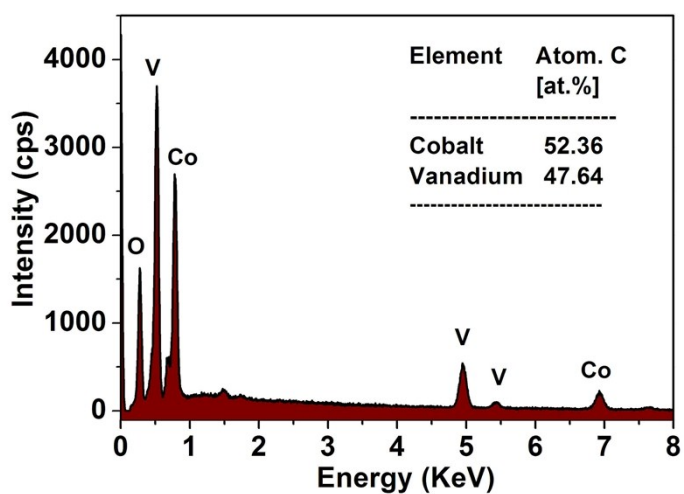


Fig. S4 EDX spectrum of the $\text{Co}_3\text{V}_2\text{O}_8$ nanoroses.

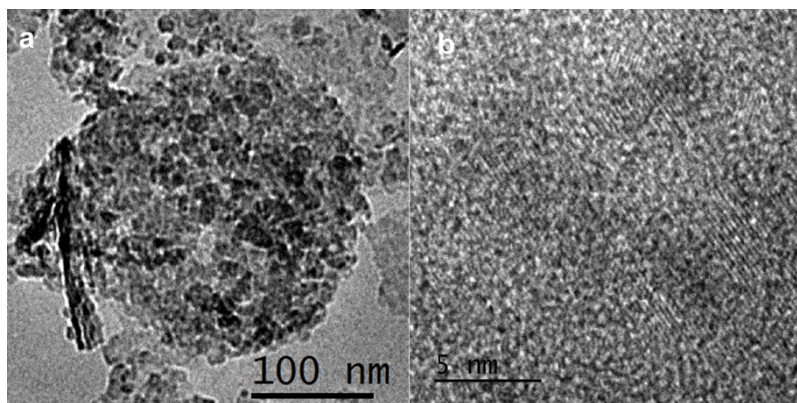


Fig. S5 (a) TEM image of an individual $\text{NiCo}_2\text{V}_2\text{O}_8$ nanoplate. (b) HR-TEM image of a fragment of $\text{NiCo}_2\text{V}_2\text{O}_8$ nanoplate.

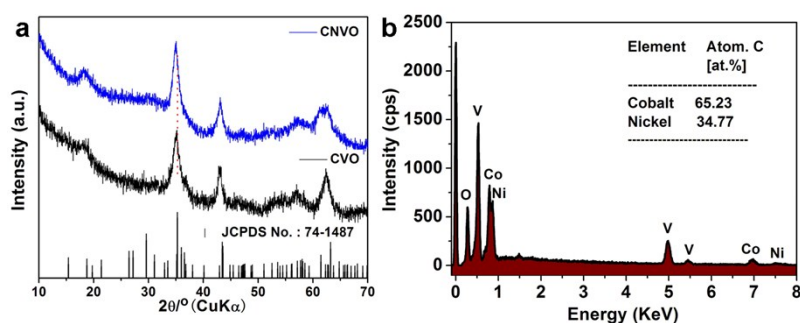


Fig. S6 (a) XRD pattern of $\text{NiCo}_2\text{V}_2\text{O}_8$ nanoplates. Vertical lines at the bottom represent the typical pattern of orthorhombic phase $\text{Co}_3\text{V}_2\text{O}_8$, the main diffractive peak moved to left, which indicated the nickel ions doped into the lattice of $\text{Co}_3\text{V}_2\text{O}_8$. (b) EDX spectrum of the $\text{NiCo}_2\text{V}_2\text{O}_8$ nanoplates.

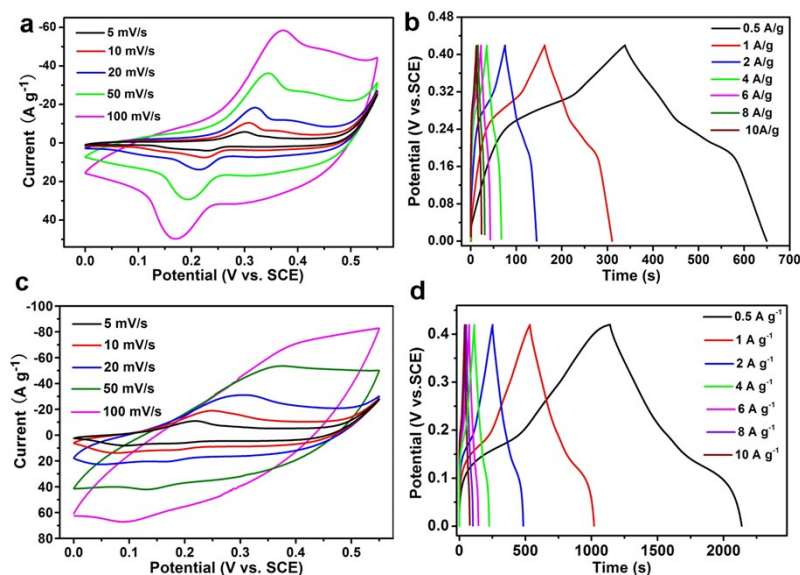


Fig. S7 Electrochemical performance characterization of $\text{Co}_3\text{V}_2\text{O}_8$ nanoroses and $\text{NiCo}_2\text{V}_2\text{O}_8$ nanoplates: (a) CV curves of $\text{Co}_3\text{V}_2\text{O}_8$ nanoroses modified electrode at various sweeping rates ranging from 5 to 100 mV s^{-1} . (b) Galvanostatic charge-discharge curves of $\text{Co}_3\text{V}_2\text{O}_8$ at different current densities. (c) CV curves of $\text{NiCo}_2\text{V}_2\text{O}_8$ nanoplates at various sweeping rates ranging from 5 to 100 mV s^{-1} . (d) Galvanostatic charge-discharge curves of $\text{NiCo}_2\text{V}_2\text{O}_8$ at different current densities.



Fig. S8 A picture of the O₂ bubbles obtained during CV test of Co₃V₂O₈ nanoroses on nickel foam.

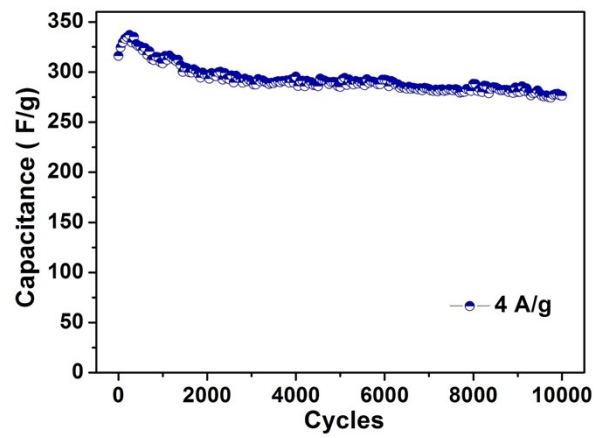


Fig. S9 The cycling performance of porous Co₃V₂O₈ nanoroses at the current density of 4A/g for 10000 cycles.

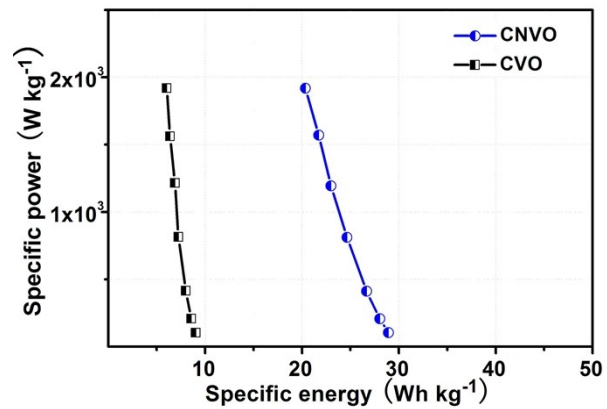


Fig. S10 Comparison of specific power vs. specific energy of porous Co₃V₂O₈ nanoroses and NiCo₂V₂O₈ nanoplates.

Electrode materials	Current density	Capacitance	Cycling stability	Ref.
Ni ₃ V ₂ O ₈ nanoflakes	0.625 A g ⁻¹	1181 F g ⁻¹	92.6% , 1000 cycles (1.25 A g ⁻¹),	39
Co ₃ V ₂ O ₈ nanoparticles	0.625 A g ⁻¹	505 F g ⁻¹	73% , 1000 cycles (1.25 A g ⁻¹)	
Co ₃ V ₂ O ₈ thin nanoplate	0.5 A g ⁻¹	739 F g ⁻¹	95.3%, 2000 cycles (0.5 A g ⁻¹)	40
CoMoO ₄ ·0.75H ₂ O nanorods	1 A g ⁻¹	285 F g ⁻¹	86.3%, 1000 cycles (1 A g ⁻¹)	47
NiMoO ₄ hierarchical nanotubes	1 A g ⁻¹	864 F g ⁻¹	71%, 1000 cycles (1 A g ⁻¹)	48
MnMoO ₄ microcrystals	2 A g ⁻¹	234 F g ⁻¹	70.5%, 1000 cycles (8 A g ⁻¹)	49
MnMoO ₄ /CoMoO ₄ nanowires	1 A g ⁻¹	187.1 F g ⁻¹	98%, 1000 cycles (3 and 20 A g ⁻¹)	50
CoMoO ₄ /MWCNTs	2 A g ⁻¹	170 F g ⁻¹	93.2%, 1000 cycles (2 A g ⁻¹)	51
NiO@CoMoO ₄ nanocomposite	1 A g ⁻¹	835 F g ⁻¹	93.2%, 1000 cycles (0.5 and 8 A g ⁻¹)	52
NiCo ₂ (PO ₄) ₂ hollow shells	4 A g ⁻¹	878.49 F g ⁻¹	84.5%, 1000 cycles (4 A g ⁻¹)	53
NH ₄ NiPO ₄ ·H ₂ O nanostructure	1.5 A g ⁻¹	1072 F g ⁻¹	95%, 3000 cycles (1.5 A g ⁻¹)	54
Cobalt–oxalate coordination polymer thin sheets	1 A g ⁻¹	702.75 F g ⁻¹	94.3%, 1000 cycles (5 A g ⁻¹)	55
Co ₃ O ₄ thin sheets	1 A g ⁻¹	1862 F g ⁻¹	99.5%, 1000 cycles (5 A g ⁻¹)	56
NiCo ₂ O ₄ @NiMoO ₄ nanomaterials	1 A g ⁻¹	2474 F g ⁻¹	95%, 2000 cycles (10 A g ⁻¹)	57
CoMoO ₄ -3D graphene hybrid	2.43 A g ⁻¹	2329 F g ⁻¹	96.36%, 100000 cycles (10 A g ⁻¹)	58
3D Co ₃ V ₂ O ₈ porous nanoroses,	1 A g ⁻¹	353.6 F g ⁻¹ ,	87.44%, 10000 cycles (4 A g ⁻¹)	Our work
2D NiCo ₂ V ₂ O ₈ nanoplates		1165.8 F g ⁻¹	68%, 7000 cycles (4 A g ⁻¹)	

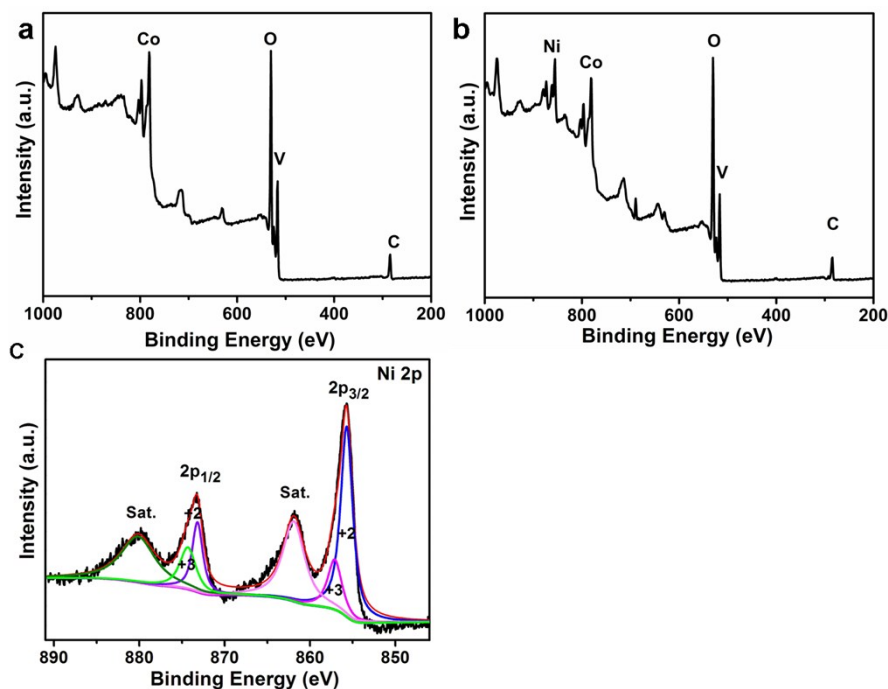


Fig. S11 (a) XPS survey spectrum of as-obtained 3D Co₃V₂O₈ nanoroses. (b) XPS spectrum of 2D porous NiCo₂V₂O₈ nanoplates. (c) The high resolution XPS spectrum of Ni 2p for NiCo₂V₂O₈ nanoplates.

Table S2 Comparison of the ratios of $\text{Co}^{3+}/\text{Co}^{2+}$ by integrating the XPS peaks of Co2p of $\text{Co}_3\text{V}_2\text{O}_8$ nanoroses and $\text{NiCo}_2\text{V}_2\text{O}_8$ nanoplates.

Sample	Areas of fitted peak				$\text{Co}^{3+}/\text{Co}^{2+}$
	Co^{3+} ($2p_{3/2}$)	Co^{2+} ($2p_{1/2}$)	Co^{3+} ($2p_{1/2}$)	Co^{2+} ($2p_{1/2}$)	
$\text{Co}_3\text{V}_2\text{O}_8$	73350.07	127651.7	61821.02	13776.25	0.96
$\text{NiCo}_2\text{V}_2\text{O}_8$	104636.8	74386.53	2653.263	54686.43	0.83

Table S3 Comparison of the ratios of $\text{O}_{\text{II}}/\text{O}$ by integrating the XPS peaks of O2p of $\text{Co}_3\text{V}_2\text{O}_8$ nanoroses and $\text{NiCo}_2\text{V}_2\text{O}_8$ nanoplates.

Sample	Areas of fitted peak				$\text{O}_{\text{II}}/\text{O}$
	O_{I}	O_{II}	O_{III}	O	
$\text{Co}_3\text{V}_2\text{O}_8$	116100.2	65000.21	35505.66	216606.07	0.30
$\text{NiCo}_2\text{V}_2\text{O}_8$	108966.4	6534.198	96442.02	211942.618	0.0308

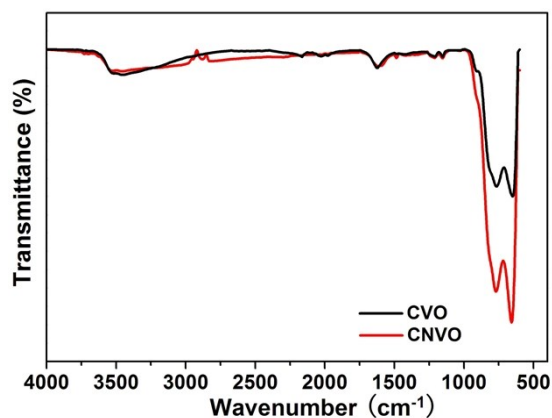


Fig. S12 IR spectra of as-obtained 3D $\text{Co}_3\text{V}_2\text{O}_8$ nanoroses and $\text{NiCo}_2\text{V}_2\text{O}_8$ nanoplates.

Faradiac efficiency of $\text{Co}_3\text{V}_2\text{O}_8$ nanoroses.

The Faradiac efficiency in OER based on a rotating ring disc electrode (RRDE), which is suitable to the OER only. The O_2 was generated on the catalyst coated glassy carbon disk and reduce by the Pt ring. (*ACS Catal.* 2016, **6**, 8069–8097; *J. Mater. Chem. A*, 2015, **3**, 6921–6928; *J. Am. Chem. Soc.* 2013, **135**, 16977–16987; *Small* 2016, **12**, 2969–2974).

A RRDE electrode (AFE729GCPT, Pine) was used to measure the Faradiac efficiency of $\text{Co}_3\text{V}_2\text{O}_8$ nanoroses. The catalytic ink was produced same as OER test, only $6.4\mu\text{L}$ ink was dropped on the disk of RRDE electrode. All the measurements were conducted under N_2 atmosphere, the disk electrode is subjected to the amperometric i-t test for 120s at a disk potential of 1.543, 1.564, 1.592, 1.619 V (vs.RHE), which corresponding to the current density of 1, 2, 5 and 10 mAcm^{-2} (Fig.7a). The ring potential is held at -0.6 V (vs. Ag/AgCl) in order to reduce O_2 to H_2O_2 . The collection efficiency (N) of the above electrode was measured in $10\text{mM K}_3\text{Fe}(\text{CN})_6$ and 0.1 M KOH aqueous solution at the various rotating speed of 100, 400, 900, 1600, 2500 rpm by liner scanning voltammetry method (Fig.7b). The scan range of the disk electrode is from 0.4 to -0.6 V (vs. Ag/AgCl) at 20 mVs^{-1} and the ring potential was kept at 0.595 V , the calculated N is ~ 0.405 . As shown in the Fig.7a, the Faradiac efficiency of $\text{Co}_3\text{V}_2\text{O}_8$ nanoroses modified RRDE electrode is 96.9%, 92.7%, 65.4% and 40.6% at 1, 2, 5 and 10 mAcm^{-2} current density, respectively.

Table S4 Comparison of the OER activity of Co₃V₂O₈ porous nanoroses and NiCo₂V₂O₈ nanoplates with previous literature.

Materials	Electrolyte	Overpotential (V@10mAcm ⁻²)	Tafel slope (mV/dec)	Ref.
CoCr ₂ O ₄	1M KOH	0.422	63.3	1
Co ₃ O ₄	1M KOH	0.400	49	2
Co ₂ N	1M KOH	0.430	80	3
Co ₃ O ₄ mesoporous nanotubes	0.1M KOH	0.390	76	4
CoFe ₂ O ₄ hollow spheres	0.1M KOH	0.450	--	5
Co ₃ O ₄ nanocubes	0.1M KOH	0.58	59	6
Co ₃ O ₄ @SiO ₂	KOH(pH=13.6)	0.529	107.7	7
NiCo double hydroxides	0.1M KOH	0.500@1mAcm ⁻²	--	8
Fe-TCA (TCA-4,4',4''-tricarboxyltriphenylamine)	1 M NaOH	0.458	87	9
Ni ₃ V ₂ O ₈ nanoflakes	1M KOH	0.429	67.37	This
Co ₃ V ₂ O ₈ porous nanoroses	1M KOH	0.391	48.34	work

1. M. Al-Mamun, X. Su, H. Zhang, H. Yin, P. Liu, H. Yang, D. Wang, Z. Tang, Y. Wang and H. Zhao, *Small*, 2016, **12**, 2866–2871.
2. M. Liao, G. Zeng, T. Luo, Z. Jin, Y. Wang, X. Kou and D. Xiao, *Electrochim. Acta*, 2016, **194**, 59–66.
3. P. Z. Chen, K. Xu, Y. Tong, X. Li, S. Tao, Z. W. Fang, W. S. Chu, X. J. Wu and C. Z. Wu, *Inorg. Chem. Front.*, 2016, **3**, 236–242.
4. H. Wang, S. F. Zhuo, Y. Liang, X. L. Han, and B. Zhang, *Angew. Chem. Int. Ed.*, 2016, **55**, 9055–9059.
5. Y. J. Xu, W. Y. Bian, J. Wu, J. H. Tian, and R. Z. Yang, *Electrochimica Acta*, 2015, **151**, 276–283.
6. Z. Chen, C. X. Kronawitter and B. E. Koel, *Phys. Chem. Chem. Phys.*, 2015, **17**, 29387–29393.
7. S. A. Khan, S. B. Khan, and A. M. Asiri, *New J. Chem.*, 2015, **39**, 5561–5569.
8. O. Diaz-Morales, I. Ledezma-Yanez, M. T. M. Koper, and F. Calle-Vallejo, *ACS Catal.*, 2015, **5**, 5380–5387.
9. B. Dhara, S. Sappati, S. K. Singh, S. Kurungot, P. Ghosh, and N. Ballav, *Dalton Trans.*, 2016, **45**, 6901–6908.
10. M. Jahan, S. Tominaka, and J. Henzie, *Dalton Trans.*, 2016, **45**, 18494–18501.

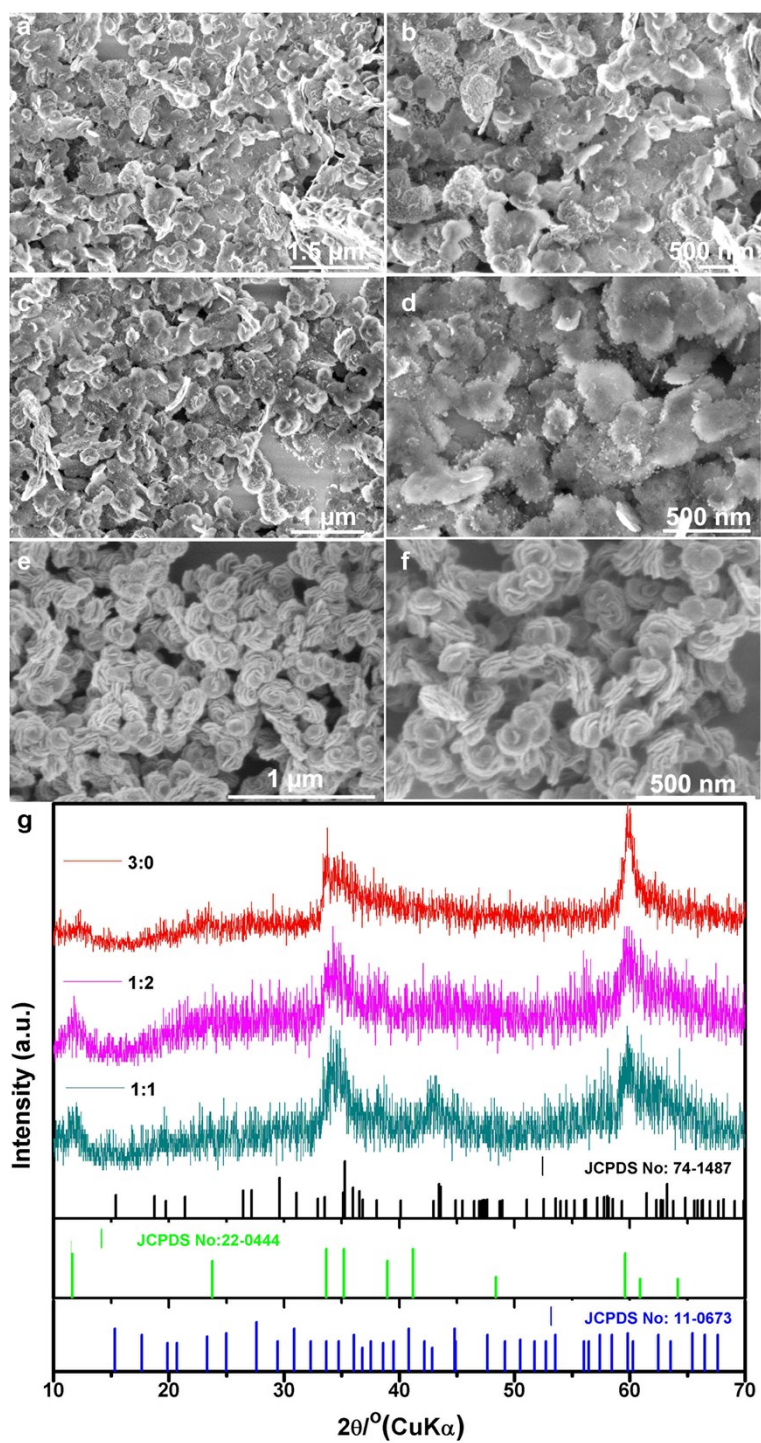


Fig.S13 SEM images of samples obtained at different ratio of Co and Ni: (a-b) 1:1, (c-d) 1:2, (e-f) 3:0, (g) the corresponding XRD curves of a-f.